

Improvement of ride quality for patient lying in ambulance with a new hydro-pneumatic suspension

Advances in Mechanical Engineering
2019, Vol. 11(4) 1–20
© The Author(s) 2019
DOI: 10.1177/1687814019837804
journals.sagepub.com/home/ade


Bohuan Tan¹ , Yang Wu¹, Nong Zhang² , Bangji Zhang¹ and Yuanchang Chen³

Abstract

Instability caused by emergency braking and steering during ambulance operation would easily lead to a sharp rise of blood pressure in patient's head, which would further cause a secondary injury to the patient. Furthermore, the vibration generated by uneven road would result in patient's nausea and deterioration of patient's condition. This article proposes a pitch–roll-interconnected hydro-pneumatic suspension system which can achieve the resistance control for pitch, roll, and bounce modes of ambulances to improve the stability and attenuate the vibration for the lying patients. The ambulance with pitch–roll-interconnected hydro-pneumatic suspension is characterized by 7 degrees of freedom dynamic model, in which the characteristics of pitch–roll-interconnected hydro-pneumatic suspension are explicitly formulated using hydrodynamic equation derivation. A motion-mode energy spectral density method is proposed to decouple the vibration energy for bounce, pitch, and roll modes in frequency domain. Subsequently, the parameter design approach incorporated with the suspension characteristic equations and motion-mode energy spectral density method is also presented to optimize the lying patient's ride comfort and ambulance's handling stability. The numerical simulation results show that the proposed pitch–roll-interconnected hydro-pneumatic suspension system can simultaneously provide pitch–roll–stiffness and damping without generating additional bounce–stiffness, resulting in superior ride comfort and handling stability compared to the conventional suspension.

Keywords

Lying patient, hydro-pneumatic suspension, ambulance, motion-mode energy, parameter design

Date received: 11 December 2018; accepted: 19 February 2019

Handling Editor: Jose Ramon Serrano

Introduction

Ambulances are important in transporting injured patients as well as providing first aid to patients. The vibration and instability of an ambulance would easily result in patient's nausea, deterioration of patient's condition, and possible death. Patients are particularly sensitive to even tiny intensity of vibration.^{1–3} When the ambulances are in operation, vibration in the lateral direction, due to the curves, would make the emergency care not easy to operate for the paramedic and even cause trauma to patient. Moreover, the subsequent pitch motion due to frequently brake and start will

generate negative foot-to-head acceleration in the lying patient, which would result in side effect, such as rapid

¹State Key Laboratory of Advanced Design and Manufacturing for Vehicle Body, Hunan University, Changsha, China

²School of Automotive and Transportation Engineering, Hefei University of Technology, Hefei, China

³Structural Dynamics and Acoustic Systems Laboratory, UMass Lowell, Lowell, MA, USA

Corresponding author:

Nong Zhang, School of Automotive and Transportation Engineering, Hefei University of Technology, Hefei 230009, China.
Email: nzhanghfut@163.com



shifting the blood to the head, reduction of venous return, and the rise of the patient's blood pressure.⁴ In order to attenuate these vibrations for lying patients, studies have focused on the suspension system of stretcher and the suspension system of vehicle body.⁵⁻⁸

So far, a limited number of studies have been carried out for the suspension system of stretcher, involving passive, semi-active, and active techniques. For instance, Yang and colleagues⁹⁻¹¹ presented a nonlinear vibration reduction stretcher system for tracked ambulance. Xu et al.¹² optimized the damping characteristic of stretchers on emergency ambulance. Pan and Zhang¹³ also investigated vibration isolation performance of ambulance stretcher. Prehn et al.¹⁴ researched the vibration and sound levels during infant transport and provided reliable improvement means. For semi-active and active system, Raine and Henderson¹⁵ investigated a semi-active pneumatic damper suspension for stretcher. Sagawa and Inooka¹⁶ carried a research on the ride quality of an actively controlled stretcher system to improve the lying patient's blood pressure variation. These studies focused on the vibration mitigation of patients lying on the stretcher and, however, did not address the issue of the vibration and stability from the perspective of paramedic. Chae and Choi¹⁷ proposed a vibration isolation bed stage with magnetorheological dampers, which can control the vibration in the stretcher as well as vibration of the seat for the paramedic. The drawbacks of this vibration isolation system, such as structural complexity and inconvenience of operation, limit its application. Actually, the simple stretcher's structure without suspension system is still very popular in practical applications due to its convenient operation during the patient transportation.

An alternative way to improve lying patient's ride quality is to design a specific suspension system of vehicle body. The advanced suspension system will enhance ride comfort and handling stability for both lying patients and paramedics. Generally, ambulances are conventionally converted from a truck or van. Their passive suspensions, though adequate for the original vehicle, are unable to meet the driving requirement of the ambulance. Semi-active and active suspensions have been adopted to improve overall dynamic performance for both handling and ride comfort,¹⁸⁻²¹ while the passive suspensions are still widely used due to inevitable limits of these semi-active/active suspensions, such as increased cost, uncertain reliability, power consumption, and inherent complexity.^{22, 23} The conventional suspension (CS) with anti-roll bars (ARBs) can improve the roll stability, while the ride comfort would be deteriorated as well.²⁴ Some advanced passive suspension systems also have been reported to enhance overall performance for both handling and ride comfort. Wu and Zhang²⁵ presented a kinetic dynamic

suspension system which can improve handling and road holding. Cao et al.²⁶ investigated the dynamic characteristics of pitch-interconnected hydro-pneumatic suspension, which indicated that the proposed suspension could provide significant benefits for improving both handling and ride qualities. Zhang et al.²⁷ proposed a roll/pitch plane hydraulically interconnected suspension (HIS) to improve roll/pitch-resistant performance without sacrificing ride comfort. Moreover, parameters optimization and sensitivity analysis were also studied for the HIS.^{28, 29} Ding et al.³⁰ proposed a roll-resistant HIS for tri-axle straight trucks, and design methodology for parameters of the HIS was also presented.

Most of the previous studies have focused on adopting various interconnected schemes to improved harmony between ride comfort and roll/pitch dynamic performance and did not involve the performance harmony among the ride comfort, roll, and pitch dynamics. For ambulances, ride comfort, roll- and pitch-resistant performance requirements are more demanding than passenger cars. However, there are only a few existing studies on both roll-pitch dynamics. For instance, Tan and Shao superficially studied the dynamic characteristic of vehicle with pitch-roll-resistant HIS system.^{31, 32} Particularly, the roll-resistant moment and pitch-resistant moments of the pitch-roll-resistant HIS are coupled together and there is a trade off among ride comfort, roll, and pitch dynamics. For example, the optimal roll-resistant performance of the vehicle is usually accompanied with excessive pitch-resistant moment, which would decrease the ride comfort of the vehicle.³¹ On the other hand, increasing the ride comfort would reduce the roll- and pitch-resistant performance. Therefore, the ride comfort, roll resistance, and pitch resistance trade off analysis and parameter design approach for pitch-roll-interconnected hydro-pneumatic suspension (PR-IHPS) are conducted in this work to balance these characters to achieve an overall optimal performance of the ambulance.

Motivated by the aforementioned discussion, this study presents a PR-IHPS system to improve stability and attenuate vibration for both lying patients and paramedics. This new suspension system can achieve enhanced cooperative control of the bounce and pitch/roll motion-modes for the ambulance. The key for improving comprehensive dynamic performance is to properly assign the bounce, pitch, and roll mode-stiffness by parameter design of PR-IHPS system. The main contributions of this article can be summarized as follows:

1. The suspension characteristics of the proposed PR-IHPS system are explicitly formulized through transfer matrix method and, furthermore, the

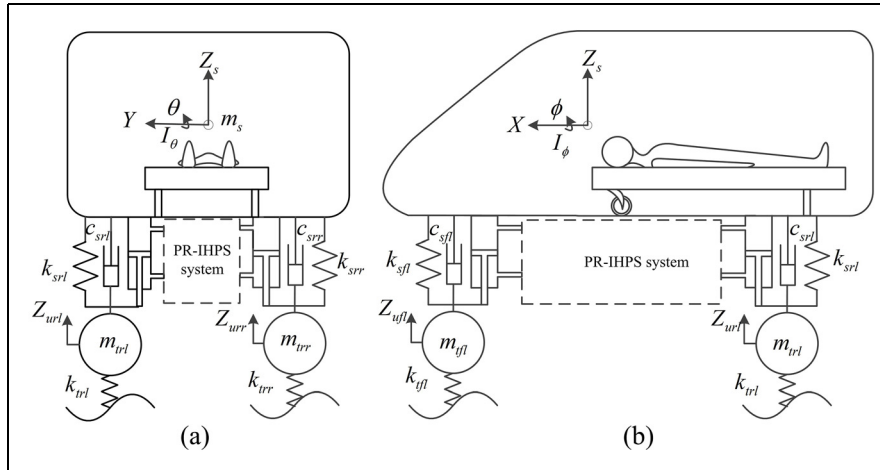


Figure 1. Schematic of a 7 DOF ambulance model: (a) rear view and (b) side view.

stiffness and damping generated by PR-IHPS are analyzed quantitatively.

- Based on the suspension characteristic analysis, the dynamic characteristics between the pitch and roll modes provided by PR-IHPS are coupled. The motion-mode energy spectral density (MESD) method is developed to decouple the vibration energy for the bounce, pitch, and roll modes in frequency domain. Then, the MESD of the decoupled modes can be obtained with different physical parameters (i.e. capacity of accumulator and pressure loss coefficient of damper valve) of PR-IHPS.
- The parameter design approach of PR-IHPS is proposed with riding and handling performance evaluation indexes (i.e. sprung mass acceleration, suspension work space, tire dynamic force, and MESD). This design procedure incorporates with the suspension characteristic equations and MESD method, so that the proposed PR-IHPS system can effectively improve the ride quality for both patients and paramedics.

The paper is organized as follows. In section “Ambulance model with PR-IHPS,” the ambulance with pitch-roll-interconnected hydro-pneumatic suspension (APR-IHPS) model is developed. Based on this model, the additional characteristics by APR-IHPS are discussed as shown in section “Characteristic analysis of PR-IHPS system.” In section “MESD method,” the MESD method for obtaining the vibration energy of each motion-mode in frequency domain is proposed, and then the equations of solving MESD of APR-IHPS are derived. Moreover, the parameter design approach for PR-IHPS system as introduced in section

“Parameter design approach of PR-IHPS system.” The simulation results and discussions are shown in section “Results and discussions.” Finally, conclusions and further work are summarized in section “Conclusion.”

Ambulance model with PR-IHPS

A 7 degrees of freedom (DOFs) ambulance model comprising a lumped sprung mass and four unsprung masses is developed, as shown in Figure 1. The sprung mass includes 3 DOFs which are translational DOF in the vertical direction, and rotational DOF in pitch and roll plane. Each lumped unsprung mass have 1 DOF which is translational freedom of motion in the vertical direction. To simplify the motion-model, the CS system is characterized by four linear spring and four viscous damping, and front and rear ARBs mounted between the sprung mass and unsprung mass are characterized by linear torsional spring. In addition, four tires are modeled using four linear springs.

In this study, a PR-IHPS system is proposed to replace front and rear ARBs to suppress pitch and roll motion of sprung mass, as schematically shown in Figure 2. In the system, actuators, described by double-acting hydraulic cylinders, are assembled between the sprung mass and unsprung mass. The diagonal hydraulic cylinders are cross-connected each other. When the ambulance turns left, positive roll motion of the sprung mass occurs, left two double-acting hydraulic cylinders are expanded while right two double-acting hydraulic cylinders are compressed. At this point, hydraulic fluid in circuits I and IV (see Figure 2) are lowly pressurized while ones in circuits II and III are highly pressurized, which together provide a roll restoring moment to prevent the roll motion of sprung mass relative to

unsprung mass. Similarly, when the ambulance turns right, the proposed PR-IHPS system can also provide a reversed roll restoring moment. The pitch motion of the sprung mass, caused by emergency braking or abrupt acceleration, has the same fundamental as the roll motion of the sprung mass, and the PR-IHPS system can also provide a pitch restoring moment. In a word, the roll and pitch motion-mode stiffness can be increased by the proposed PR-IHPS system. In terms of bounce and articulation motion-modes, compression and extension of the hydraulic cylinders would make hydraulic fluid in circuits flow into extension chamber from compression chamber, which makes the fluid pressure almost unchanged. It means that the PR-IHPS system can only provide additional damping forces, but additional stiffness is scarcely offered in both bounce and articulation modes.

Equations for vehicle

The equations of motion for the vehicle model can be derived, in which the hydraulic forces are regarded as external forces

$$\mathbf{M}\ddot{\mathbf{x}} + \mathbf{C}\dot{\mathbf{x}} + \mathbf{K}\mathbf{x} = \mathbf{F}_h + \mathbf{F}_w \quad (1)$$

where $\mathbf{x} = [Z_s \ \theta \ \phi \ Z_{ufL} \ Z_{ufR} \ Z_{urL} \ Z_{urR}]^T$ is displacement vector and $\mathbf{F}_w = [0 \ 0 \ 0 \ k_{zfl}z_{gfl} \ k_{zfr}z_{gfr} \ k_{zrl}z_{grl} \ k_{zrr}z_{grr}]^T$ is road disturbance input vector. \mathbf{F}_h is hydraulic forces due to the pressure in the cylinder chambers and it can be expressed as $\mathbf{F}_h = \mathbf{D}_p\mathbf{P}$, where the pressure matrix $\mathbf{P} = [P_{flT} \ P_{flB} \ P_{frT} \ P_{frB} \ P_{rlT} \ P_{rlB} \ P_{rrT} \ P_{rrB}]^T$ and the area coefficient matrix \mathbf{D}_p can be written as

$$\mathbf{D}_p = \begin{bmatrix} S_{flT} & -S_{flB} & S_{frT} & -S_{frB} & S_{rlT} & -S_{rlB} & S_{rrT} & -S_{rrB} \\ -aS_{flT} & aS_{flB} & -aS_{frT} & aS_{frB} & bS_{rlT} & -bS_{rlB} & bS_{rrT} & -bS_{rrB} \\ t_f S_{flT} & -t_f S_{flB} & -t_f S_{frT} & t_f S_{frB} & t_r S_{rlT} & -t_r S_{rlB} & -t_r S_{rrT} & t_r S_{rrB} \\ -S_{flT} & S_{flB} & 0 & 0 & 0 & 0 & 0 & 0 \\ 0 & 0 & -S_{frT} & S_{frB} & 0 & 0 & 0 & 0 \\ 0 & 0 & 0 & 0 & -S_{frB} & S_{rlB} & 0 & 0 \\ 0 & 0 & 0 & 0 & 0 & 0 & -S_{rrT} & S_{rrB} \end{bmatrix} \quad (2)$$

Equations for PR-IHPS system

N Zhang²⁷ proposed a transfer matrix method to develop the equations of the fluid subsystem, and this method is employed for the modeling of PR-IHPS system. Each fluid circuit is made up of one nitrogen-filled diaphragm accumulator, one three-way junction, three damper valves, and a few fluid pipelines components, as illustrated in Figure 2. Thus, the relationship between flow and pressure in the circuit can be determined by a sequence of multiplications of the involved fluid component impedance matrices

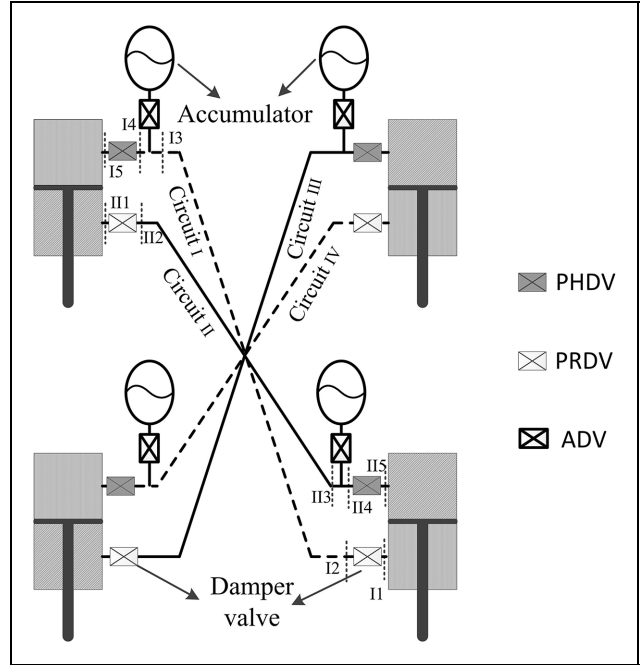


Figure 2. A schematic of PR-IHPS system.

$$\begin{bmatrix} P_D^k \\ Q_D^k \end{bmatrix} = {}^{k5}\mathbf{T}_{k4}^v \times {}^{k4}\mathbf{T}_{k3}^t \times {}^{k3}\mathbf{T}_{k2}^p \times {}^{k2}\mathbf{T}_{k1}^v \begin{bmatrix} P_U^k \\ Q_U^k \end{bmatrix} \quad (3)$$

$$= \begin{bmatrix} T_{11}^k & T_{12}^k \\ T_{21}^k & T_{22}^k \end{bmatrix} \begin{bmatrix} P_U^k \\ Q_U^k \end{bmatrix}$$

The fluid element lumped-parameter model is applied to these components. Therefore, the hydrody-

amic equations of pipeline fluid element can be expressed as

$$P_U - P_D = R_p Q + I_p \dot{Q} \quad \text{and} \quad Q_U - Q_D = C_p \dot{P} \quad (4)$$

where $P = (P_U + P_D)/2$ and $Q = (Q_U + Q_D)/2$ are the mean pressure and mean flow in pipeline fluid element, respectively. Substituting P and Q into equation (4), and then the Laplace transform is applied with zero initial conditions, which can be written as

$$\begin{aligned} \begin{bmatrix} P_D \\ Q_D \end{bmatrix} &= \begin{bmatrix} \frac{I_p s + R_p + 4s^{-1}/C_p}{-I_p s - R_p + 4s^{-1}/C_p} & -\frac{4(I_p s + R_p)s^{-1}/C_p}{-I_p s - R_p + 4s^{-1}/C_p} \\ -\frac{4}{-I_p s - R_p + 4s^{-1}/C_p} & \frac{I_p s + R_p + 4s^{-1}/C_p}{-I_p s - R_p + 4s^{-1}/C_p} \end{bmatrix} \begin{bmatrix} P_U \\ Q_U \end{bmatrix} \\ &= {}^D\mathbf{T}_U^p \begin{bmatrix} P_U \\ Q_U \end{bmatrix} \end{aligned} \quad (5)$$

For the damper valve and accumulator with the three-way junction and damper valve (ATJDV) components, the hydrodynamic equations can be written as

$$\begin{bmatrix} P_D \\ Q_D \end{bmatrix} = \begin{bmatrix} 1 & -Z_H \\ 0 & 1 \end{bmatrix} \begin{bmatrix} P_U \\ Q_U \end{bmatrix} = {}^D\mathbf{T}_U^v \begin{bmatrix} P_U \\ Q_U \end{bmatrix} \quad (6)$$

$$\begin{bmatrix} P_D \\ Q_D \end{bmatrix} = \begin{bmatrix} 1 & 0 \\ -1/(sC_a) & 1 \end{bmatrix} \begin{bmatrix} P_U \\ Q_U \end{bmatrix} = {}^D\mathbf{T}_U^t \begin{bmatrix} P_U \\ Q_U \end{bmatrix} \quad (7)$$

where C_a is the capacity of a gas-filled diaphragm accumulator and it can be expressed by $C_a = P_p V_p / \gamma \bar{P}^2$.

Substituting equations (5)–(7) into equation (3), and expanding the expressions to all circuits, the relationship between pressure and flow can be rewritten as

$$\mathbf{P} = \mathbf{T}(s)\mathbf{Q} \quad (8)$$

where $\mathbf{Q} = [Q_{fIT} \ Q_{fIB} \ Q_{fIT} \ Q_{fIB} \ Q_{rIT} \ Q_{rIB} \ Q_{rrT} \ Q_{rrB}]^T$ is flow state vector, and $\mathbf{T}(s)$ is the total impedance matrix of the PR-IHPS system and can be expressed as

$$\mathbf{T}(s) = \begin{bmatrix} -\frac{T_{22}^I}{T_{21}^I} & 0 & 0 & 0 & 0 & 0 & 0 & 0 & \frac{1}{T_{21}^I} \\ 0 & \frac{T_{11}^{II}}{T_{21}^{II}} & 0 & 0 & 0 & 0 & 0 & \frac{T_{12}^{II}T_{21}^{II} - T_{11}^{II}T_{22}^{II}}{T_{21}^{II}} & 0 \\ 0 & 0 & -\frac{T_{22}^{III}}{T_{21}^{III}} & 0 & 0 & 0 & \frac{1}{T_{21}^{III}} & 0 & 0 \\ 0 & 0 & 0 & \frac{T_{11}^{IV}}{T_{21}^{IV}} & \frac{T_{12}^{IV}T_{21}^{IV} - T_{11}^{IV}T_{22}^{IV}}{T_{21}^{IV}} & 0 & 0 & 0 & 0 \\ 0 & 0 & 0 & \frac{1}{T_{21}^{IV}} & -\frac{T_{22}^{IV}}{T_{21}^{IV}} & 0 & 0 & 0 & 0 \\ 0 & 0 & \frac{T_{12}^{III}T_{21}^{III} - T_{11}^{III}T_{22}^{III}}{T_{21}^{III}} & 0 & 0 & \frac{T_{11}^{III}}{T_{21}^{III}} & 0 & 0 & 0 \\ 0 & \frac{1}{T_{21}^{II}} & 0 & 0 & 0 & 0 & 0 & -\frac{T_{22}^{II}}{T_{21}^{II}} & 0 \\ \frac{T_{12}^I T_{21}^I - T_{11}^I T_{22}^I}{T_{21}^I} & 0 & 0 & 0 & 0 & 0 & 0 & 0 & \frac{T_{11}^I}{T_{21}^I} \end{bmatrix} \quad (9)$$

Boundary equations for the vehicle and PR-IHPS

The relative motion between the piston head and rod cylinder results in the change of volume flow in the cylinder chambers, and vice versa. The interaction between the relative motion and volume flow rate forms the coupled boundary for conventional ambulance and PR-IHPS system. It should be noted that the compression of the fluid and the cross-line leakage in the cylinder chambers can be ignored for small-amplitude oscillations under low pressure. Therefore, the interaction can be described as $q = Sv$, where S is the piston surface areas, and q and v are piston flow and relative

velocity, respectively. Then, the relationship can be applied to four-cylinder chambers

$$\begin{aligned} \mathbf{Q}(t) &= \mathbf{D}_m \dot{\mathbf{x}}(t) \\ &= \begin{bmatrix} -S_{fIT} & aS_{fIT} & -t_f S_{fIT} & S_{fIT} & 0 & 0 & 0 & 0 \\ -S_{fIB} & aS_{fIB} & -t_f S_{fIB} & S_{fIB} & 0 & 0 & 0 & 0 \\ -S_{fIT} & aS_{fIT} & t_f S_{fIT} & 0 & S_{fIT} & 0 & 0 & 0 \\ -S_{fIB} & aS_{fIB} & t_f S_{fIB} & 0 & S_{fIB} & 0 & 0 & 0 \\ -S_{rIT} & -bS_{rIT} & -t_r S_{rIT} & 0 & 0 & S_{rIT} & 0 & 0 \\ -S_{rIB} & -bS_{rIB} & -t_r S_{rIB} & 0 & 0 & S_{rIB} & 0 & 0 \\ -S_{rrT} & -bS_{rrT} & t_r S_{rrT} & 0 & 0 & 0 & S_{rrT} & 0 \\ -S_{rrB} & -bS_{rrB} & t_r S_{rrB} & 0 & 0 & 0 & 0 & S_{rrB} \end{bmatrix} \dot{\mathbf{x}}(t) \end{aligned} \quad (10)$$

Integrated equations for ambulance with PR-IHPS

Based on equations (1), (8), and (10), the integrated equations can be written as

$$\mathbf{M}\ddot{\mathbf{x}} + \mathbf{C}\dot{\mathbf{x}} + \mathbf{K}\mathbf{x} = \mathbf{D}_p \mathbf{T}(s)\mathbf{D}_m \dot{\mathbf{x}} + \mathbf{F}_w \quad (11)$$

The impedance matrix $\mathbf{T}(s)$ can be obtained by equation (9), which depends on the physical parameters of the fluid components. Then, the equations of motion of

coupling system, applying the Laplace transform with zero initial conditions, can be rewritten as

$$[s^2 \mathbf{M} + s \mathbf{C} \underbrace{-s \mathbf{D}_p \mathbf{T}(s) \mathbf{D}_m}_{\mathbf{Z}_{PR-IHPS}} + \mathbf{K}] \mathbf{X}(s) = \mathbf{F}_w \quad (12)$$

Then, equation (12) can be expressed in state-space form as

$$s \tilde{\mathbf{X}}(s) = \mathbf{A}(s) \tilde{\mathbf{X}}(s) + \mathbf{B} \mathbf{U}(s) \quad (13)$$

where $\tilde{\mathbf{X}}(s)$ and $\mathbf{U}(s)$ are the Laplace transformation of the system state vector ($\tilde{\mathbf{X}}(s) = L([\mathbf{x}^T \dot{\mathbf{x}}^T]^T)$) and the disturbance input vector, respectively. The characteristic matrix and $\mathbf{A}(s)$ input coefficient matrix \mathbf{B} can be written as

$$\mathbf{A}(s) = \begin{bmatrix} \mathbf{0} & \mathbf{I} \\ -\mathbf{M}^{-1}\mathbf{K} & -\mathbf{M}^{-1}(\mathbf{C} - \mathbf{D}_p\mathbf{T}(s)\mathbf{D}_m) \end{bmatrix} \quad \text{and} \\ \mathbf{B} = \begin{bmatrix} \mathbf{0} \\ -\mathbf{M}^{-1}\mathbf{F}_w \end{bmatrix} \quad (14)$$

Stiffness characteristic

The stiffness characteristic matrix $\mathbf{K}_{PR-IHPS}$ can be written as

$$\mathbf{K}_{PR-IHPS} = \frac{1}{C_P + C_a} \underbrace{\begin{bmatrix} \mathbf{K}_b (3 \times 3) & \mathbf{K}_{bw} (3 \times 4) \\ \mathbf{K}_{bw}^T (4 \times 3) & \mathbf{K}_w (4 \times 4) \end{bmatrix}}_{\mathbf{K}_{co}} S_r T^2 \quad (16)$$

where \mathbf{K}_{co} is area coefficient matrix, in which \mathbf{K}_b and \mathbf{K}_w are the area coefficient matrices of stiffness for sprung mass and unsprung mass, respectively, and \mathbf{K}_{bw} is the coupled area coefficient matrix between sprung mass and unsprung. Introducing area ratio variables $\Lambda_{(m,n)}$ and $\Omega_{(m,n)}$, the area coefficient matrices can be written as

$$\mathbf{K}_b = \begin{bmatrix} 2(\Lambda_{(0,0)}^2 + \Omega_{(0,0)}^2) & -2(\Lambda_{(1,0)}\Lambda_{(0,0)} + \Omega_{(1,0)}\Omega_{(0,0)}) & 0 \\ \text{Symmetry} & 2(\Lambda_{(1,0)}^2 + \Omega_{(1,0)}^2) & 0 \\ & & 2(\Lambda_{(0,1)}^2 + \Omega_{(0,1)}^2) \end{bmatrix} \quad (17)$$

$$\mathbf{K}_{bw} = \begin{bmatrix} -\mu\Lambda_{(0,0)} - \eta_f\mu\Omega_{(0,0)} & -\mu\Lambda_{(0,0)} - \eta_f\mu\Omega_{(0,0)} & \eta_r\Lambda_{(0,0)} + \Omega_{(0,0)} & \eta_r\Lambda_{(0,0)} + \Omega_{(0,0)} \\ \mu\Lambda_{(1,0)} + \eta_f\mu\Omega_{(1,0)} & \mu\Lambda_{(1,0)} + \eta_f\mu\Omega_{(1,0)} & -\eta_r\Lambda_{(1,0)} - \Omega_{(1,0)} & -\eta_r\Lambda_{(1,0)} - \Omega_{(1,0)} \\ -\mu\Lambda_{(0,1)} - \eta_f\mu\Omega_{(0,1)} & \mu\Lambda_{(0,1)} + \eta_f\mu\Omega_{(0,1)} & -\eta_r\Lambda_{(0,1)} - \Omega_{(0,1)} & \eta_r\Lambda_{(0,1)} + \Omega_{(0,1)} \end{bmatrix} \quad (18)$$

$$\mathbf{K}_w = \begin{bmatrix} \mu^2(\eta_f^2 + 1) & 0 & 0 & -\mu(\eta_r + \eta_f) \\ \mu^2(\eta_f^2 + 1) & -\mu(\eta_r + \eta_f) & 0 & 0 \\ \text{Symmetry} & \eta_r^2 + 1 & 0 & 0 \\ & & \eta_r^2 + 1 & 0 \end{bmatrix} \quad (19)$$

Characteristic analysis of PR-IHPS system

Based on additional characteristic matrix $\mathbf{Z}_{PR-IHPS}$, the dynamic characteristics of PR-IHPS can be studied. For simplicity consideration, the whole system is assumed to be symmetry, which means the components installed in either circuit possess the same physical and hydraulic parameters. The cross-sectional area ratio between the bottom and top of the front or rear cylinder η_i ($i = f, r$) and the ratio between the rear and front top cylinders μ are introduced, which can be written as $\eta_i = S_{iB}/S_{iT}$ and $\mu = S_{fT}/S_{rT}$. It is noted that the additional characteristic matrix is a N -order polynomial on Laplace operator s , which can be expanded as

$$\mathbf{Z}_{PR-IHPS} = (s^2\mathbf{M}_{PR-IHPS} + s\mathbf{C}_{PR-IHPS} + \mathbf{K}_{PR-IHPS})\mathbf{X} \\ = \mathbf{M}_{PR-IHPS}\ddot{\mathbf{x}} + \mathbf{C}_{PR-IHPS}\dot{\mathbf{x}} + \mathbf{K}_{PR-IHPS}\mathbf{x} \quad (15)$$

The second and third terms on the right of equation represent the additional damping and stiffness characteristics by the PR-IHPS system, respectively. Based on these matrixes, the stiffness and damping characteristics of PR-IHPS will be explicitly described in next sections.

where $\Lambda_{(m,n)} = a^m t_f^n \mu - (-1)^{m+n} b^m t_r^n \eta_r$ and $\Omega_{(m,n)} = a^m t_f^n \eta_f \mu - (-1)^{m+n} b^m t_r^n$ ($m = 0, 1; n = 0, 1$)

Equation (16) clearly shows that the additional stiffness is inversely proportional to sum of liquid capacitance and accumulator's capacity and also depends on the cross-sectional areas. Further investigation of equation (17) can demonstrate that:

1. The vertical stiffness for sprung mass is determined by vertical area ratio factor $\mathbf{K}_b(1,1)$ and vertical-pitch coupled area ratio factor $\mathbf{K}_b(1,2)$. It can be found that the PR-IHPS system does not provide vertical stiffness for sprung mass when the areas of hydraulic cylinders meet $\Lambda_{(0,0)} = 0$ and $\Omega_{(0,0)} = 0$ which indicate that the front and rear cylinders are oppositely installed. In addition, the vertical motion and pitch motion are decoupled completely for PR-IHPS system under this condition.
2. The pitch stiffness and roll stiffness for sprung mass, respectively, depend on the area ratio factor $\mathbf{K}_b(2,2)$ and $\mathbf{K}_b(3,3)$, which are a quadratic function of the area of hydraulic cylinder. It clearly indicates that $\mathbf{K}_b(1,1)$ is much less than $\mathbf{K}_b(2,2)$ and $\mathbf{K}_b(3,3)$, which means that the PR-

IHPS only generates small vertical spring rate and provides great pitch angular and roll angular spring rate.

3. The motions of front-left wheel and rear-right wheel are intercoupled by area ratio factor $-\mu(\eta_r + \eta_f)$, as well as front-right wheel and rear-left wheel. Meanwhile, the area coefficient matrix \mathbf{K}_w indicates that the PR-IHPS system increases the vertical stiffness of unsprung mass.

Damping characteristic

The additional damping depends on liquid capacitance of pipeline and loss coefficients of valves. Actually, the liquid resistances resulted from pipelines are much smaller than that produced by damper valves. Thus, only the valve-produced damping is discussed in this section.

The valves can be classified as piston head damper valve (PHDV), piston rod damper valve (PRDV), and accumulator damper valve (ADV), as illustrated in Figure 2. Based on equation (15), the damping matrix $\mathbf{C}_{PR-IHPS}$ can be expressed as

$$\mathbf{C}_{PR-IHPS} = Z_A \mathbf{K}_{co} + Z_H \begin{bmatrix} \mathbf{C}_{b(0)} & \mathbf{C}_{bw(0)} \\ \mathbf{C}_{bw(0)}^T & \mathbf{C}_{w(0)} \end{bmatrix} S_{rT}^2 + Z_R \begin{bmatrix} \mathbf{C}_{b(2)} & \mathbf{C}_{bw(2)} \\ \mathbf{C}_{bw(2)}^T & \mathbf{C}_{w(2)} \end{bmatrix} S_{rT}^2 \quad (20)$$

The submatrices \mathbf{C}_b and \mathbf{C}_w are the area coefficient matrices of damping for sprung mass and unsprung mass, respectively, and \mathbf{C}_{bw} is the coupled area coefficient matrix. They can be expressed as

$$\mathbf{C}_{b(i)} = \begin{bmatrix} 2(\eta_f^i \mu^2 + \eta_r^i) & -2(a\eta_f^i \mu^2 - b\eta_r^i) & 0 \\ 2(a^2 \eta_f^i \mu^2 + b^2 \eta_r^i) & 0 & 0 \\ \text{Symmetry} & & 2(t_f^2 \eta_f^i \mu^2 + t_r^2 \eta_r^i) \end{bmatrix} \quad (21)$$

$$\mathbf{C}_{bw(i)} = \begin{bmatrix} -\eta_f^i \mu^2 & -\eta_f^i \mu^2 & -\eta_r^i & -\eta_r^i \\ a\eta_f^i \mu^2 & a\eta_f^i \mu^2 & -b\eta_r^i & -b\eta_r^i \\ -t_f \eta_f^i \mu^2 & t_f \eta_f^i \mu^2 & -t_r \eta_r^i & t_r \eta_r^i \end{bmatrix} \quad (22)$$

$$\mathbf{C}_{w(i)} = \text{diag}(\eta_f^i \mu^2, \eta_f^i \mu^2, \eta_r^i, \eta_r^i) \quad (23)$$

As shown in equation (20), the first item on the right of the equation indicates the additional damping characteristic matrix generated by ADVs. In addition, the second and third items are determined by PHDVs and PRDVs. More details are shown as follows:

1. Equation (20) clearly shows that the damping characteristic matrix $Z_A \mathbf{K}_{co}$ is similar to the stiffness characteristic matrix $\mathbf{K}_{PR-IHPS}$. It indicates that for ADVs, the effects of the cross-sectional

areas on the damping characteristic are the same with the effects on the additional stiffness characteristic.

2. Equation (22) and (23) indicates that both PHDVs and PRDVs can generate the additional vertical, pitch, and roll motion damping for sprung mass. The motion between the vertical and pitch are coupled by area ratio factor $-2(a\eta_f^i \mu^2 - b\eta_r^i)$. In addition, the motions between unsprung mass, unlike ADVs, are decoupled for the damping characteristic generated by PHDVs and PRDVs, as shown in equation (23).

In sum, the PR-IHPS system can provide the pitch and roll stiffness simultaneously and achieve damping adjustment to the specified motion by changing pressure loss coefficients of damper valves. Remarkably, the pitch and roll stiffness are coupled and depend on the same set of parameters. In order to reasonably design the coupled stiffness and damping, the MESD method is introduced to decoupled the vibration energy of each mode in the next section.

MESD method

A motion-mode energy method has been proposed to quantify the energy contribution of each motion-mode to vehicle dynamics in real time.^{33,34} In this method, the motion energy of three vehicle body-dominated modes (bounce, pitch, and roll) which contribute most to vehicle ride quality can be described. Based on this method, MESD method is developed to achieve the decomposition of motion-mode energy in the frequency domain. Therefore, the MESD of each motion-mode can be independently obtained using the proposed method, and then the influence of parameters of PR-IHPS system on the MESD can be discovered. This is the key point to design appropriate parameters for PR-IHPS system.

MESD

Based on the theory of random vibration, the motion energy of single DOF in the frequency domain under random road input can be quantified by acceleration power spectral density (PSD) which is defined as

$$Y(f) = |H(f)_{\ddot{y}-q}|^2 G_q(f) = H(f)_{\ddot{y}-q}^* G_q(f) H(f)_{\ddot{y}-q} \quad (24)$$

where $H(f)_{\ddot{y}-q}$ is the transfer function (TF) from road displacement input to acceleration response of vehicle body. $G_q(f)$ is the road disturbance input PSD and it can be written as $G_q(f) = G_0 n_0^w f^{-w} V^{w-1}$ where the exponent w denotes the energy distribution for the wavelength, $G_0 = 64 \times 10^{-6} \text{ m}^3/\text{Hz}$ is the roughness coefficient of the average road surface, and V is the

forward speed. The symbols * and T denote complex conjugate and matrix transpose, respectively. Similarly, the PSD responses of road disturbance at four wheels can be described as

$$\hat{\mathbf{Y}} = \mathbf{H}^* S_w \mathbf{H}^T \quad (25)$$

where S_w is the road disturbance input PSD for four wheels. \mathbf{H} is the TF matrices from road input vector to outputs and can be written as

$$\mathbf{H} = \bar{\mathbf{C}}(s\mathbf{I} - \mathbf{A}(s))^{-1} \mathbf{B} + \bar{\mathbf{D}} \quad (26)$$

in which $\bar{\mathbf{C}}$ and $\bar{\mathbf{D}}$ are the output coefficient matrix and the feed-forward matrix, respectively.

With respect to equation (13), the eigenvalue matrix Θ and the eigenvector matrix Π of the integrated system can be calculated

$$\Theta = \text{diag}(\tilde{\Lambda} \quad \tilde{\Lambda}^*) \quad \text{and} \quad \Pi = \begin{bmatrix} \Psi & \Psi^* \\ \Psi \tilde{\Lambda} & \Psi^* \tilde{\Lambda}^* \end{bmatrix} \quad (27)$$

where $\tilde{\Lambda}$ and Ψ are system eigenvalue and eigenvector matrices, respectively, given as

$$\tilde{\Lambda} = \text{diag}(\lambda_1, \lambda_2, \dots, \lambda_7) \quad \text{and} \quad \Psi = [\varphi_1, \varphi_2, \dots, \varphi_7] \quad (28)$$

where λ_j and φ_j ($j = 1, 2, \dots, 7$) are the j th eigenvalue and the corresponding eigenvector, respectively, and they can be calculated using the approximate optimization method after the linearization.³¹ Then, using modal theory,^{35, 36} the state vector component $\tilde{\mathbf{x}}_j$ for j th mode in the physical coordinate can be represented by coordinate transformations between physical coordinate and modal coordinate

$$\tilde{\mathbf{x}}_j = \underbrace{\{[\mathbf{II}]_{(all,j)}[\mathbf{II}^{-1}]_{(j,all)} + [\mathbf{II}^*]_{(all,j)}[(\mathbf{II}^{-1})^*]_{(j,all)}\}}_{\mathbf{T}_j} \tilde{\mathbf{x}} \quad (29)$$

in which (all, j) and (j, all) are j row and j column of the matrix, respectively. \mathbf{T}_j is 14×14 dimensional transformation matrix of the j th order motion-mode. Then, the output responses of j th motion-mode \mathbf{Y}_{mj} can be formulated as

$$\mathbf{Y}_{mj} = \bar{\mathbf{C}} \tilde{\mathbf{x}}_j + \bar{\mathbf{D}} \mathbf{U}_j \quad (30)$$

Substituting equation (29) into equation (30) yields

$$\mathbf{Y}_{mj} = \underbrace{(\bar{\mathbf{C}} \mathbf{T}_j (s\mathbf{I} - \mathbf{A})^{-1} \mathbf{B} + \bar{\mathbf{D}} \mathbf{T}_j)}_{\mathbf{H}_{mj}} \mathbf{U} \quad (31)$$

where \mathbf{H}_{mj} is defined as the TF matrix of j th order mode. Then, the corresponding output response \mathbf{Y}_{mj} under road input vector \mathbf{U} can be calculated. It is worth

to point out that the overall output response $\hat{\mathbf{Y}}$ and the TF matrix \mathbf{H} can be decomposed into seven response component matrices \mathbf{Y}_{mj} and seven TF component matrices \mathbf{H}_{mj} . Thus, the output PSD response for each motion-mode under four-wheel random road inputs can be developed as

$$\mathbf{Y}_j = \mathbf{H}_{mj}^* S_w \mathbf{H}_{mj}^T \quad (32)$$

The diagonal elements of \mathbf{Y}_j represent the j th modal direct spectral densities of the output variables in \mathbf{Y}_{mj} . Then, the kinetic energy spectrum density D_j^K and potential energy spectrum density D_j^P stored in the j th motion-mode can be defined as

$$D_j^K = \frac{1}{2} \mathbf{M}_D \mathbf{Y}_j^V \quad (33)$$

$$D_j^P = \frac{1}{2} \mathbf{K}_D \mathbf{Y}_j^D \quad (34)$$

Furthermore, the summation of the energy for each motion-mode is defined as

$$D_j = D_j^K + D_j^P \quad (35)$$

MESD for APR-IHPS

In order to calculate the MESD of system, the equivalent stiffness of the system and the corresponding elastic deformation in equation (34) must be clear. It is well known that the spring stiffness coefficients in vehicle system depend on a single constant and can be obtained directly by measurement. However, the stiffness generated by PR-IHPS is determined by multiple parameters such as capacity of accumulator, cross-section area of hydraulic cylinder. It is important to obtain the equivalent stiffness of four hydraulic cylinders to calculate the MESD of APR-IHPS.

The four hydraulic cylinder output forces applied on the sprung mass and unsprung mass can be divided into damping force and elastic force using equation (11) as

$$\begin{aligned} \mathbf{F}_H &= s \mathbf{D}_h \mathbf{T}(s) \mathbf{D}_m \mathbf{X} = (s \mathbf{C}_{FH} + \mathbf{K}_{FH}) \mathbf{X} \\ &= (\mathbf{Z}_A \mathbf{S}_K + \mathbf{Z}_H \mathbf{S}_H + \mathbf{Z}_R \mathbf{S}_R) \dot{\mathbf{x}} + \frac{1}{C_p + C_a} \mathbf{S}_K \mathbf{x} \end{aligned} \quad (36)$$

where \mathbf{D}_h , \mathbf{S}_K , \mathbf{S}_H , \mathbf{S}_R are the area matrices associated with the corresponding cylinder chambers and they are defined as follows

$$\mathbf{D}_h = \begin{bmatrix} S_{flT} & -S_{flB} & 0 & 0 & 0 & 0 & 0 & 0 \\ 0 & 0 & S_{frT} & -S_{frB} & 0 & 0 & 0 & 0 \\ 0 & 0 & 0 & 0 & S_{rlT} & -S_{rlB} & 0 & 0 \\ 0 & 0 & 0 & 0 & 0 & 0 & S_{rrT} & -S_{rrB} \end{bmatrix} \quad (37)$$

$$\mathbf{S}_K = \begin{bmatrix} \mathbf{K}_{bw}^T (4 \times 3) & \mathbf{K}_w (4 \times 4) \end{bmatrix} \mathcal{S}_r T^2 \quad (38)$$

$$\mathbf{S}_H = \begin{bmatrix} \mathbf{C}_{bw(0)}^T & \mathbf{C}_{w(0)} \end{bmatrix} \mathcal{S}_r T^2 \quad (39)$$

$$\mathbf{S}_R = \begin{bmatrix} \mathbf{C}_{bw(2)}^T & \mathbf{C}_{w(2)} \end{bmatrix} \mathcal{S}_r T^2 \quad (40)$$

Thus, the equivalent relative deformations of four cylinders are expressed as $\mathbf{S}_K \mathbf{x}$, and the equivalent velocity flowing through ADV, PHDV, and PRDV is respectively defined as $\mathbf{S}_K \dot{\mathbf{x}}$, $\mathbf{S}_H \dot{\mathbf{x}}$, and $\mathbf{S}_R \dot{\mathbf{x}}$. Their outputs under road excitations for each motion-mode can be calculated using equation (31), and the corresponding response \mathbf{Y}_{mj} and output coefficient matrix $\bar{\mathbf{C}}$ can be rewritten as

$$\begin{aligned} \mathbf{Y}_{mj} &= [\mathbf{Y}_{Kj} \quad \mathbf{Y}_{Aj} \quad \mathbf{Y}_{Hj} \quad \mathbf{Y}_{Rj}]^T \quad \text{and} \quad \bar{\mathbf{C}} \\ &= [\mathbf{S}_K \quad s\mathbf{S}_K \quad s\mathbf{S}_H \quad s\mathbf{S}_R]^T \end{aligned} \quad (41)$$

Furthermore, the corresponding PSD \mathbf{Y}_j^K , \mathbf{Y}_j^A , \mathbf{Y}_j^H , and \mathbf{Y}_j^R can be obtained by equation (32). Therefore, neglecting liquid capacitance and mass of PR-IHPS system, the total kinetic energy spectrum density D_j^K and potential energy spectrum density D_j^P stored in the j th motion-mode for the APR-IHPS can be redefined as follows

$$D_j^K = \frac{1}{2} \text{diag}(\mathbf{M}) \mathbf{Y}_j^V \quad (42)$$

$$D_j^P = \frac{1}{2} (\mathbf{K}_D \mathbf{Y}_j^D + \mathbf{K}_{HP} \mathbf{Y}_j^K) \quad (43)$$

in which $\mathbf{Y}_j^V = [\dot{Z}_s \quad \dot{\theta} \quad \dot{\phi} \quad \dot{Z}_{ufr} \quad \dot{Z}_{ur} \quad \dot{Z}_{urr}]_j^T$ is the velocity PSD vector for the j th motion-mode, $\mathbf{K}_{HP} = [1/(C_p + C_a) \quad 1/(C_p + C_a) \quad 1/(C_p + C_a) \quad 1/(C_p + C_a)]^T$ is the stiffness coefficient vector of PR-IHPS system, and $\mathbf{Y}_j^K = [Y_{sfl} \quad Y_{sfr} \quad Y_{srl} \quad Y_{srr}]_j^T$ is the PSD output of j th motion-mode corresponding to $\mathbf{S}_K \mathbf{x}$. Then, the total MESD of j th motion-mode can be obtained by equation (35).

Parameter design approach of PR-IHPS system

Performance evaluation indexes

The stiffness/damping characteristic alterations of suspension systems are embodied in the responses of the ambulance subject to random excitations. In this study, the weighted acceleration for recumbent position (WARP), the suspension working space (SWS), and the tire dynamic force (TDF) are adopted to evaluate the dynamic performance of the ambulance. The PSD responses of these indexes can be calculated by equation (25), and then corresponding root mean square (RMS) values (i.e. σ_{SWS} and σ_{TDF}) can be obtained by Simpson integration. Particularly, the RMS value of WARP R_I reflected the ride comfort can be calculated

according to international standard ISO 2631—evaluation of human exposure to whole-body vibration in recumbent position.³⁷ For SWS and TDF evaluations, the dynamic SWS and TDF coefficients are respectively defined as $\gamma(\sigma_{SWS}) = \sigma_{SWS}/D_0$ and $\gamma(\sigma_{TDF}) = \sigma_{TDF}/F_0$, respectively. Generally, an increase in the roll/pitch stiffness is beneficial to improve the stability of the ambulance while having a negative impact on ride comfort. Therefore, the motion energy on the pitch and roll modes, especially the pitch mode effecting the patient's blood pressure, should be considered after incorporating PR-IHPS system. It can be found from equations (16) and (17) that the pitch and mode-stiffness/-damping generated by PR-IHPS system are coupled via the suspension parameters, such as the sectional areas and the capacities/loss coefficients. Thus, the decoupled MESDs of pitch and roll modes, in this study, are also adopted as evaluation indexes to design the parameters of PR-IHPS.

Design approach

The design process can be divided into three parts which are hydraulic cylinder sectional area design, equivalent stiffness design, and damping design, as shown in Figure 3. Generally, softer bounce-stiffness is beneficial for improvement of ride comfort because it can reduce the vertical acceleration levels of the sprung mass, while the stiffer stiffness in pitch and roll modes are helpful to enhance handling stability. Based on equation (17), the cross-sectional area of the hydraulic cylinders are the key parameters effecting the stiffness characteristic of the PR-IHPS. Therefore, the hydraulic sectional areas are designed to make both pitch and roll stiffness to be maximum and bounce-stiffness minimum. For this purpose, adjusting the area variables to maximize $\mathbf{K}_{b(2,2)}$ and $\mathbf{K}_{b(3,3)}$, and minimize $\mathbf{K}_{b(1,1)}$ and $\mathbf{K}_{b(1,2)}$ as much as possible.

Another component that affects the stiffness characteristics is accumulator's capacity C_a which can be calculated as $C_a = P_p V_p / \gamma \bar{P}^2$. It is the key parameters determining the stiffness characteristics—the larger the capacity, the softer the suspension, and the smaller the capacity, the stiffer the suspension. In order to ensure the low vibration energy in pitch and roll modes, the corresponding MESDs are solved with different capacities. Subsequently, considering the ride comfort and handling requirements (see section “The capacity of accumulator” for details), the feasible range of the capacity design is determined.

For the damping design, the objective for the optimization is to minimize the WARP (R_I), MESD (D_{Pitch} and D_{Roll}), SWS ($\gamma(\sigma_{SWS})$), and TDF ($\gamma(\sigma_{TDF})$). Once the feasible capacity $C_{ai} \in [C_{a0}, C_{a1}, \dots, C_{am}]$ is determined, the optimal loss coefficients can be obtained. Then, the capacity is updated to further optimize the

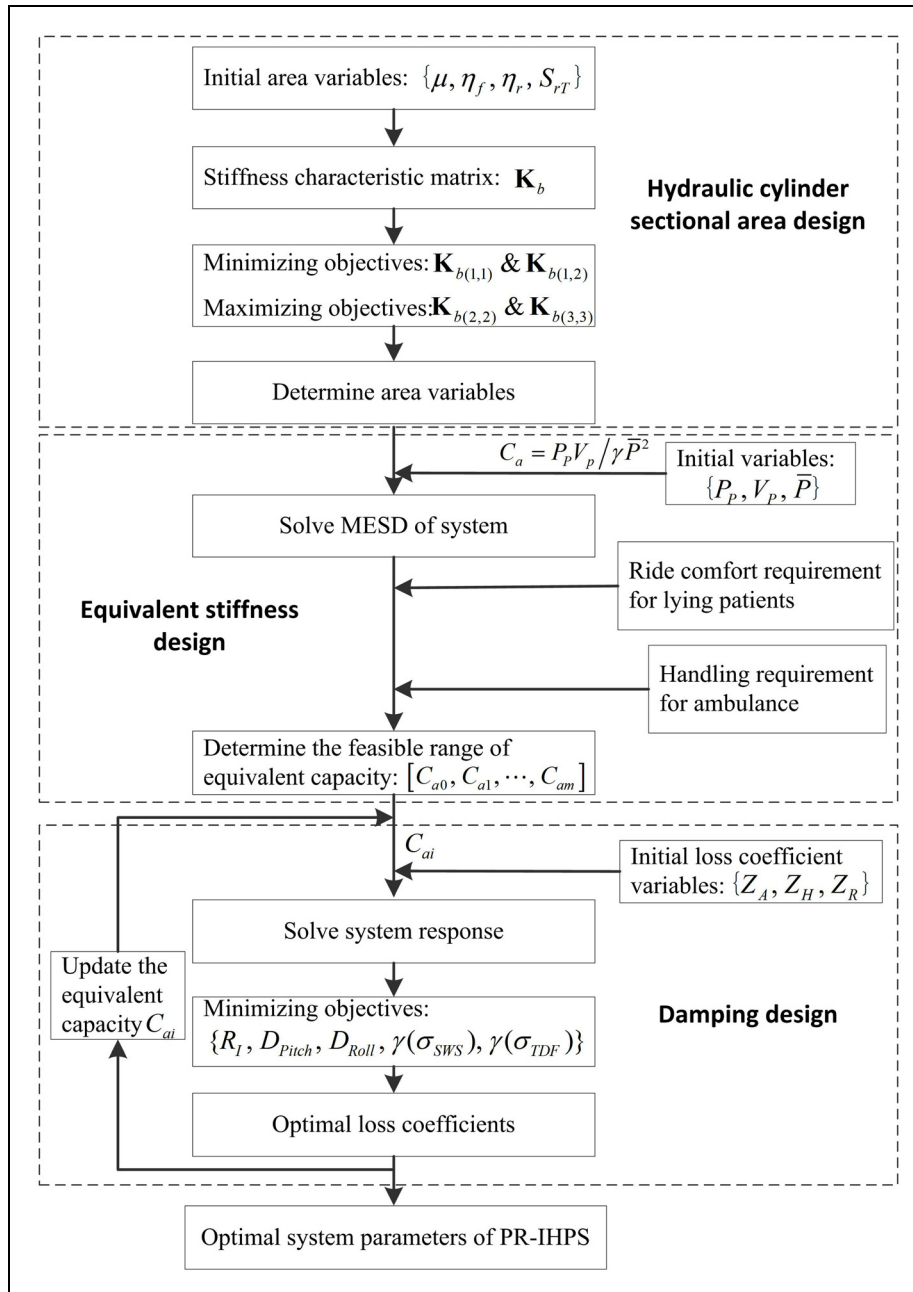


Figure 3. Block diagram of parametric design for PR-IHPS system.

loss coefficients. Finally, the optimal system parameters of PR-IHPS can be selected eclectically in different capacities with the corresponding loss coefficients.

Results and discussions

Two models, ambulance with conventional suspension (ACS) and APR-IHPS, are applied to investigate the dynamic performance and motion-mode energy. A set of mechanical and hydraulic parameters used in the two models are presented in Appendix 2.

Dynamic analysis and MESD responses

In order to estimate the dynamic performance, the PSD responses to random excitation inputs are taken into consideration. The comparison between ACS and APR-IHPS is performed under a constant vehicle speed of 50 km/h.

Based on modal analysis,³⁸ the mode frequencies corresponding to pitch and roll modes significantly increase by 32.26% and 20.89%, respectively, after incorporating the PR-IHPS system, while mode frequency of bounce slightly decreases by 5.17% as shown

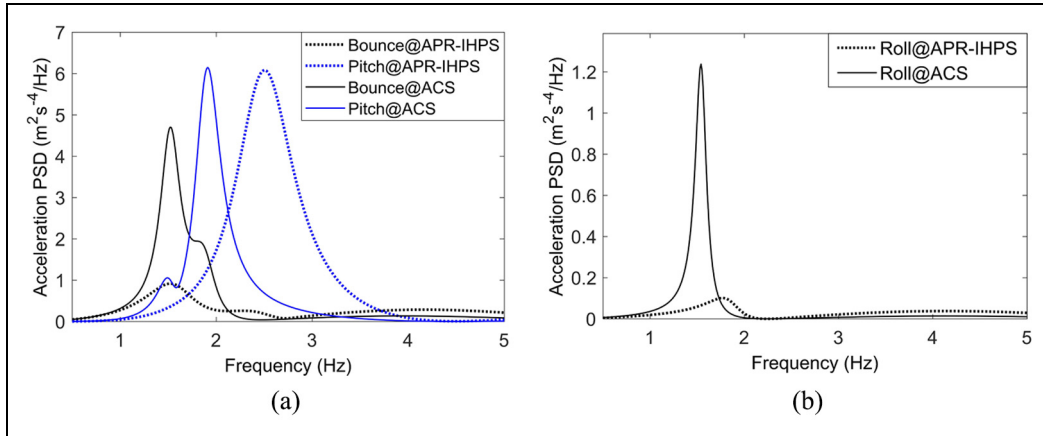


Figure 4. Comparison in terms of acceleration PSD responses: (a) bounce and pitch angular and (b) roll angular.

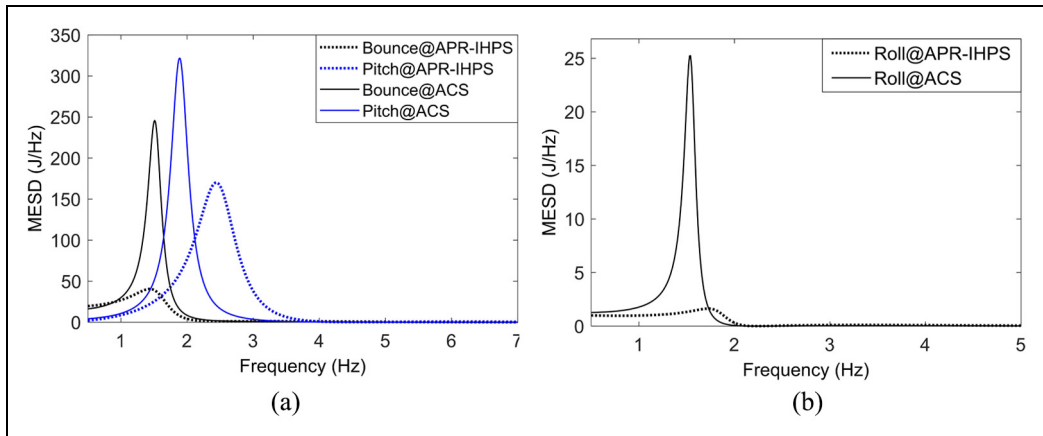


Figure 5. Comparison in terms of MESDs: (a) bounce and pitch and (b) roll.

in Appendix 3. For the articulation mode, the mode frequency remarkably decreases by 27.26%. In addition, the vibration decay rate of each mode is significantly increased. Figure 4 shows the comparison in terms of PSD responses between ACS and APR-IHPS. Obviously, the proposed PR-IHPS system effectively reduces the resonance peak values for the bounce, pitch, and roll motions. These results illustrate that the PR-IHPS system can enhance handling performance without compromising the ride comfort.²⁷ Particularly, the low articulation modal frequency indicates that PR-IHPS system can improve the road holding ability for an off-road condition.²⁵

The MESDs of the vehicle body-dominated modes are shown in Figure 5. The PR-IHPS system significantly reduces the peak values of the MESD response curves, which indicates that the vibration energy is greatly suppressed by PR-IHPS system. The peak frequencies corresponding to MESD curves are consistent with the resonance frequencies of the vehicle body-dominated modes. Furthermore, the comparison of

RMS values of the MESD between APR-IHPS and ACS is illustrated in Figure 6. It is noted that the PR-IHPS system can effectively suppress the motion energy of the ambulance.

As stated above, the PR-IHPS system has the ability to improve the overall operating performance of an ambulance. In order to achieve the optimal overall performance, the key parameters of PR-IHPS system will be analyzed and designed in the next section.

Parametric analysis for PR-IHPS system

Based on the parameter design approach shown in section “Parameter design approach of PR-IHPS system,” the parameters of PR-IHPS system are discussed in terms of the cross-sectional areas, the accumulator’s capacity, and the valves’ loss coefficients.

Cross-sectional areas of hydraulic cylinders. Based on equation (17), the area ratio η_r is first set to a fixed value of

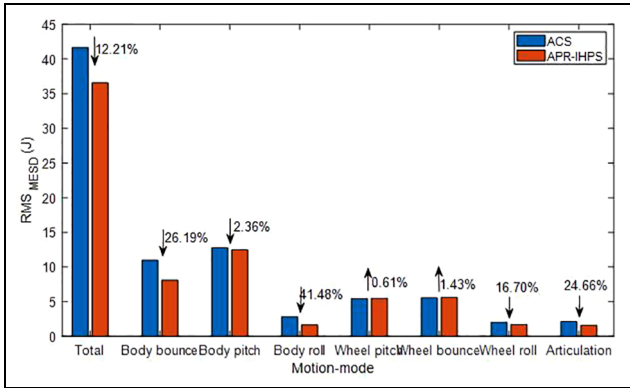


Figure 6. Comparison of RMS values of MESD between ACS and APR-IHPS.

0.6 to investigate the effects of μ and η_f on the stiffness characteristics produced by PR-IHPS system. Figure 7 denotes that the area ratio η_f and bounce area factor $\mathbf{K}_{b(1,1)}$ are in a quadratic function relationship when the area ratio μ is certain. The red point-dashed curve represents the set of minimum values for all quadratic functions, which shows that this curve is also a quadratic function and reaches its minimal value when $\mu = 0.6$ and $\eta_f = 1.66$. At this minimal value point, the area ratios meet $\Lambda_{(0,0)} = 0$ and $\Omega_{(0,0)} = 0$, which indicates that the bounce-stiffness is not provided. For the roll area factor $\mathbf{K}_{b(3,3)}$, it has similar result with the $\mathbf{K}_{b(2,2)}$.

Figure 8 shows the minimum lines with different rear area ratios η_r in $\mathbf{K}_{b(2,2)}-\mathbf{K}_{b(1,1)}$ coordinate system. It is noted that the minimum values of all lines are equal to “zero.” The identical area point (IAP) curve is the set of the IAPs on all minimum lines as shown by dashed line in Figure 8. Therefore, the region above the IAP curve represents installation in the same direction between front and rear cylinders. On the contrary, the region below the IAP curve refers to installation in the opposite direction. Therefore, in order to obtain minimal bounce-stiffness and great pitch/roll stiffness, the area ratios in lower-right region which represents piston rod upward installation for rear cylinders and piston rod downward installation for front cylinders are the optimal choice. To meet the engineering requirements, three ratios $\eta_f = 0.625$, $\eta_r = 1.6$, and $\mu = 1.6$ are adopted in this study.

The capacity of accumulator. In the design of van, there is handling performance index that the suspension system needs to meet, which is the roll angle of sprung mass cannot exceed 2.5° (0.0436 rad) when the lateral acceleration reaches 5 m/s^2 .³⁹ In this study, the handling requirement of APR-IHPS is also considered to design the capacity of accumulator. Based on equation (36), the static nonlinear stiffness curves of PR-IHPS system

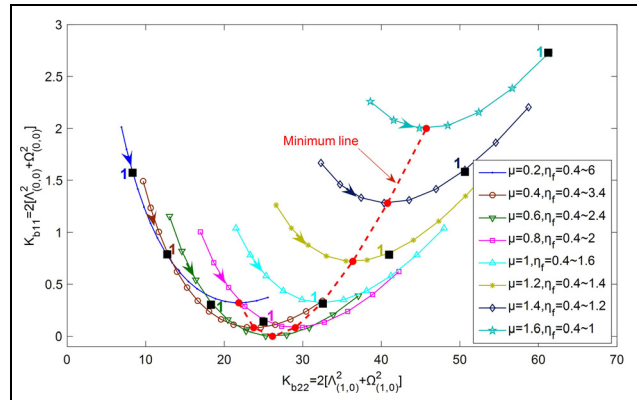


Figure 7. The effects of area ratios in terms of μ and η_f on $\mathbf{K}_{b(1,1)}$ and $\mathbf{K}_{b(2,2)}$, where the square symbol “■” denotes “ $\eta_f = 1$ ” which is called as the identical area point (IAP).

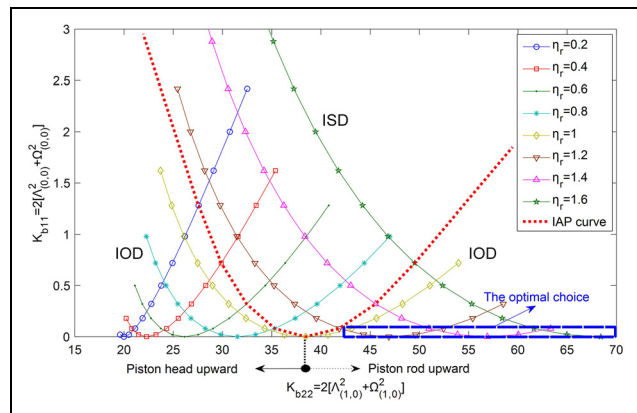


Figure 8. The minimum line with different η_r .

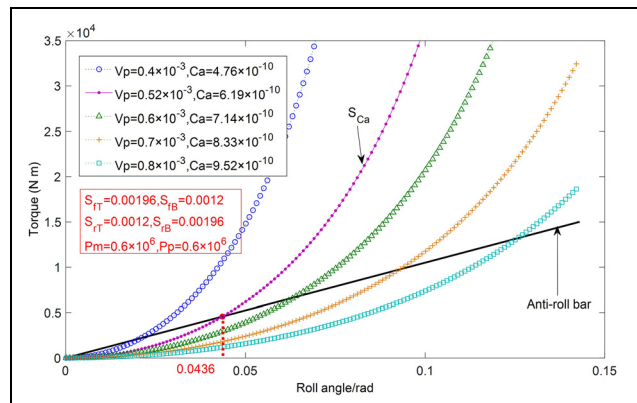


Figure 9. The static stiffness of PR-IHPS.

can be obtained as shown in Figure 9. It indicates that the stiffness of PR-IHPS system increases with the decrease of accumulator’s capacity C_a . Furthermore, in the case of a relatively small roll angle, the PR-IHPS

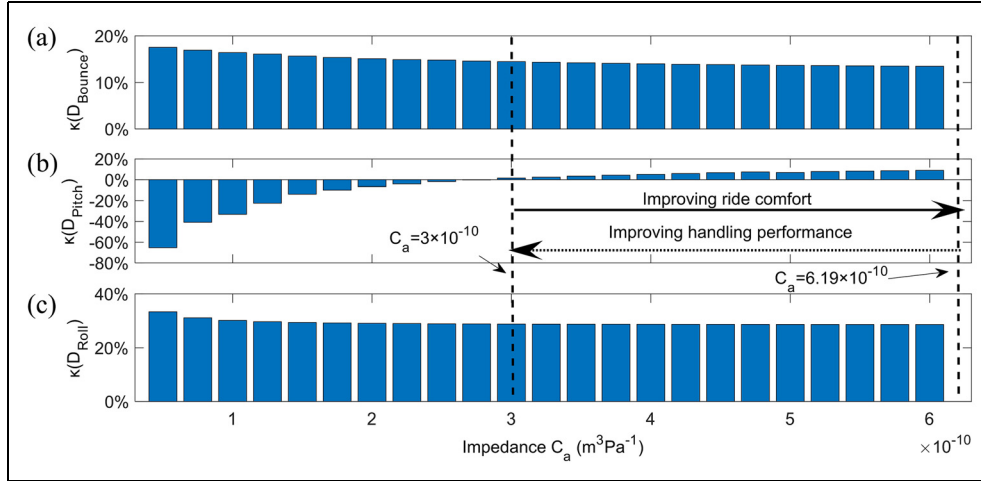


Figure 10. The relative errors of MESDs: (a) bounce, (b) pitch, and (c) roll.

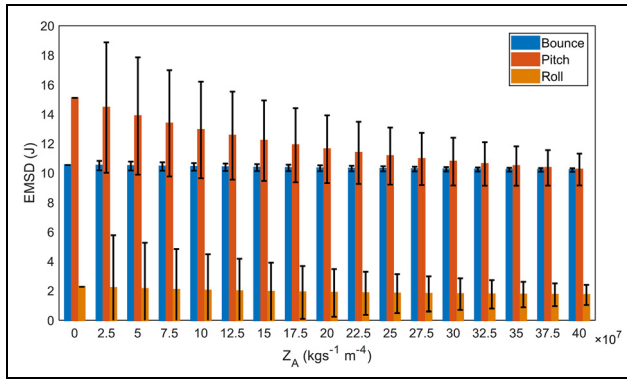


Figure 11. The effects of Z_A on MESDs.

system provides less stiffness than the ARB. At the range of relatively large roll angle, the stiffness of the PR-IHPS system is greater than that of the ARB. For the CS that has been designed, the ARB provides a torque of 4578 N m when the roll angle of sprung mass reaches 0.0436 rad. The torque provided by PR-IHPS system also needs to meet this requirement, that is, $S_{Ca} = 6.19 \times 10^{-10} \text{ m}^3/\text{Pa}$, as demonstrated in Figure 9. Therefore, accumulator's capacity needs to satisfy a constraint condition which is $C_a \leq 6.19 \times 10^{-10} \text{ m}^3/\text{Pa}$ for improving the handling performance of APR-IHPS.

Figure 10 shows the comparison of MESDs between APR-IHPS and ACS with the change of C_a , and the relative error factor $\kappa(D_j)$ is formulized as $\kappa(D_j) = (D_j^{ACS} - D_j^{APR-IHPS})/D_j^{ACS}$ ($j = \text{Bounce, Pitch, roll}$), where D_j^{ACS} and $D_j^{APR-IHPS}$ are the MESDs corresponding to ACS and APR-IHPS, respectively. Figure 10(a) and (c) indicates that the bounce and roll MESDs of APR-IHPS reduce by nearly 20% and 40% compared to ACS, respectively. For pitch motion-mode, the MESD decreases with the

increase of C_a . The MESD of APR-IHPS is less than that of ACS when C_a exceeds $3 \times 10^{-10} \text{ m}^3/\text{Pa}$. It proves that the PR-IHPS system can effectively suppress the vibration energy both in the bounce, pitch, and roll modes, but the excessively small capacity C_a will lead to significant increase of MESD in the pitch modes. To improve the ride comfort, these three MESDs are required to be as low as possible. Thus, the accumulator's capacity needs to meet the constraint conditions for ride comfort, that is, $C_a \geq 3 \times 10^{-10}$. Taking into consideration of the constraint conditions of handling, the capacity can be designed to be in the range from 3×10^{-10} to $6.19 \times 10^{-10} \text{ m}^3/\text{Pa}$. In this range, high capacity can improve the handling performance, while low capacity can enhance the ride comfort.

The loss coefficients of damper valves. The effects of the loss coefficients on the MESDs of vehicle body-dominated modes are investigated. The loss coefficient Z_A is first considered assuming $Z_H = 0$ and $Z_R = 0$. The variation gradient of index is adopted and can be defined as $G = [(V_P - V_L)/V_L]$, where V_P and V_L are the present value and previous value, respectively, as shown by symbol "I" in Figure 11. The height of this symbol represents the magnitude of the gradient. It can be seen from Figure 11 shows that the loss coefficient has a significant negative correlation with the MESD of pitch mode, as well as roll mode, while has a subtle influence on the bounce mode. It indicates that the ADV can effectively suppress the vibration energy of pitch and roll modes, while it has slight influence on the vibration energy of bounce mode.

To analysis the loss coefficients Z_H and Z_R further, Figure 12 shows the contour plots associate with $Z_A = 3.5 \times 10^8 \text{ kg s}^{-1} \text{ m}^{-4}$ in Z_H-Z_R coordinate system.

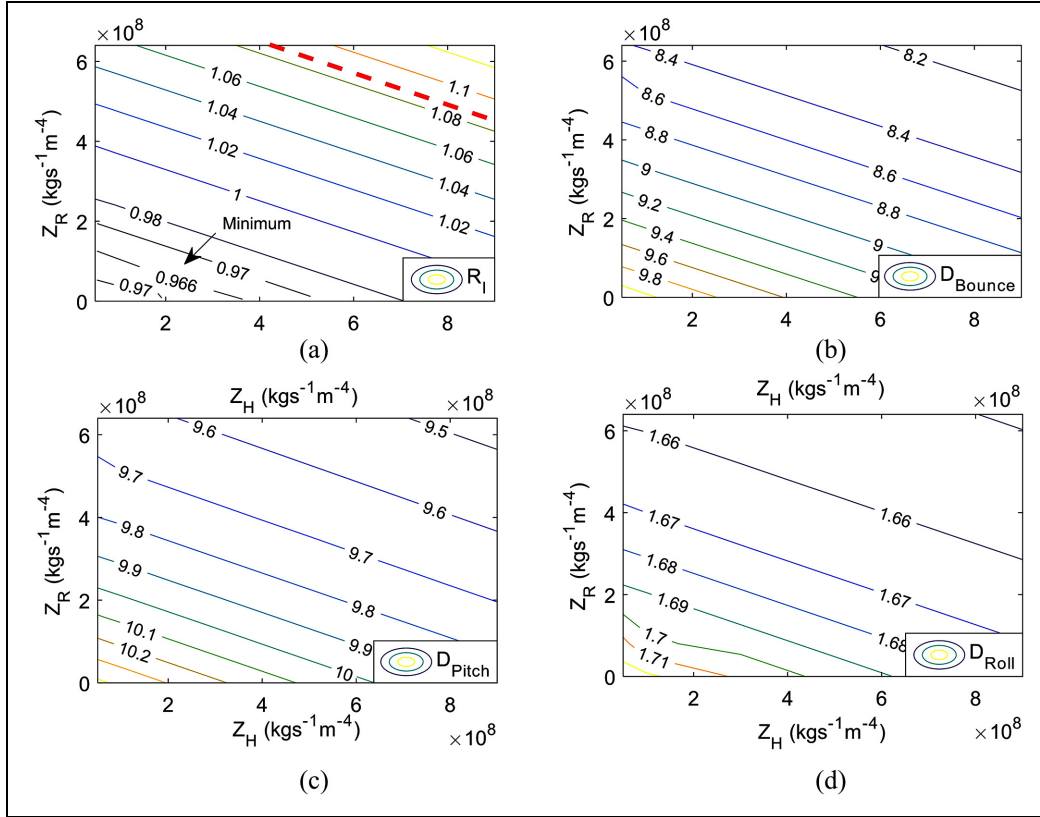


Figure 12. The contour plots with respect to valuation index when $Z_A = 3.5 \times 10^8 \text{ kg s}^{-1} \text{ m}^{-4}$: (a) R_I , (b) D_{Bounce} , (c) D_{Pitch} , and (d) D_{Roll} .

Figure 12(a) indicates that the minimum value that is $R_I = 0.966 \text{ m/s}^2$ can be obtained, when the values of Z_H and Z_R are in the range of $0-0.364 \times 10^8 \text{ kg s}^{-1} \text{ m}^{-4}$ and $0-1.18 \times 10^8 \text{ kg s}^{-1} \text{ m}^{-4}$, respectively. For the ACS, the comfort index is equal to 1.0849 m/s^2 , as shown by the red-dotted line in Figure 12(a). The ride comfort of APR-HIS is obviously better than that of ACS by designing appropriate loss coefficients. The region below the red-dotted line is defined as workable region. Figure 12(b)–(d) shows the MESD contour plots of bounce, pitch, and roll modes, respectively, which indicates that MESDs of APR-IHPS are less than that of ACS (10.95, 12.77, and 2.82 J). In sum, the design of loss coefficients can reach the desired ride comfort. In addition, the loss coefficients have positive effects on MESDs of pitch and roll modes.

Figure 13(a) and (b) shows the contour plots of front SWS index $\gamma(\sigma_{SWS}^F)$ and rear SWS index $\gamma(\sigma_{SWS}^R)$ in terms of Z_H and Z_R when $Z_A = 3.5 \times 10^8 \text{ kg s}^{-1} \text{ m}^{-4}$. For APR-IHPS, $\gamma(\sigma_{SWS}^F)$ and $\gamma(\sigma_{SWS}^R)$ decrease when Z_H/Z_R increases; both of them are less than those of ACS (0.3306 and 0.2179). Figure 13(c) and (d) shows the contour plots of front TDF index $\gamma(\sigma_{TDF}^F)$ and rear TDF index $\gamma(\sigma_{TDF}^R)$ which points out that the $\gamma(\sigma_{TDF}^F)$ and $\gamma(\sigma_{TDF}^R)$ decrease first and then increase as the

Z_H/Z_R increases, and the corresponding minimum values are 0.329 and 0.4481, respectively. Similarly, the TDF indexes of APR-IHPS are less than that those of ACS (0.3784 and 0.2649) as well. Finally, the desired loss coefficients can be obtained by weighing these conflicting performances comprehensively.

Parameters design results

Based on the parameter design approach described above, the optimal parameter set for PR-IHPS system is obtained, as shown in Table 1. To evaluate the optimization, the performance indexes of the three configurations, ACS, original (unoptimized) APR-IHPS, and optimized APR-IHPS, are compared in Table 2. In addition, the pitch angular displacement (PAD) and roll angular displacement (RAD) of sprung mass are also considered to further evaluate the stability for the lying patient. These indexes are normalized³⁰ and compared using a radar-type chart, as shown in Figure 14, which indicates that the overall performance of the optimized APR-IHPS has significantly improved. Most performances indexes of the original APR-IHPS are better than ACS except the ride comfort factor and TDF. The reason for these performance degradation is

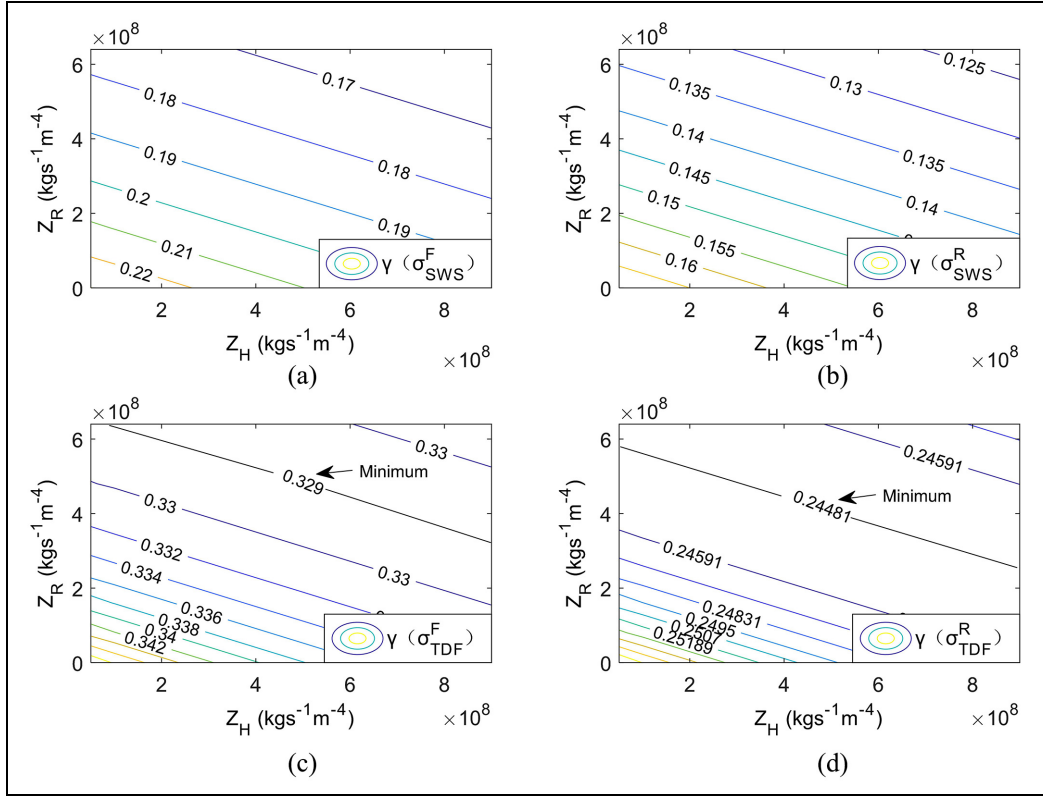


Figure 13. The contour plots with respect to SWS and TDF when $Z_A = 3.5 \times 10^8 \text{ kg s}^{-1} \text{ m}^{-4}$: (a) σ_{SWS}^F , (b) σ_{SWS}^R , (c) σ_{TDF}^F , and (d) σ_{TDF}^R .

Table 1. The optimized parameter set for the PR-IHPS system.

Parameters	D_T (m)	D_B (m)	\bar{P} (MPa)	P_p (MPa)	V_p (m ³)	Z_A (kg s ⁻¹ m ⁻⁴)	Z_H (kg s ⁻¹ m ⁻⁴)	Z_R (kg s ⁻¹ m ⁻⁴)
PR-IHPS	5×10^{-2}	4×10^{-2}	1.8	0.5	6.3×10^{-4}	3×10^8	7×10^8	7×10^8
Optimized PR-IHPS	5×10^{-2}	3.06×10^{-2}	1.5	1.12	7.8×10^{-4}	3.5×10^8	4.7×10^8	3.8×10^8

PR-IHPS: pitch-roll-interconnected hydro-pneumatic suspension.

Table 2. Comparison of the performance among ACS, original APR-IHPS, and optimized APR-IHPS.

Performance indexes	R_f (m s ⁻²)	σ_{PAD} (rad)	σ_{RAD} (rad)	D_{Pitch} (J)	D_{Roll} (J)	$\gamma(\sigma_{SWS}^F)$	$\gamma(\sigma_{SWS}^R)$	$\gamma(\sigma_{TDF}^F)$	$\gamma(\sigma_{TDF}^R)$
ACS	1.085	0.014	12.771	0.007	2.816	0.331	0.218	0.378	0.265
Original APR-IHPS	1.181	0.011	12.196	0.004	1.648	0.187	0.114	0.414	0.288
Optimized APR-IHPS	1.024	0.010	9.717	0.005	1.664	0.183	0.138	0.330	0.245

ACS: ambulance with conventional suspension; APR-IHPS: ambulance with pitch-roll-interconnected hydro-pneumatic suspension.

that the pitch stiffness generated by PR-IHPS system is excessive, so that the acceleration of the sprung mass and the dynamic forces applied on the unsprung masses increases significantly.

Figure 15 shows that the total motion energy for the optimal APR-IHPS is reduced by 16.58% compared to ACS, which is more than 12.21% of the

original APR-IHPS, which indicates that the motion energy can be optimized by the parameter design for the PR-IHPS system. Particularly, the body pitch MESD of optimal APR-IHPS is obviously lower than that of original APR-IHPS, while the other MESD is comparable. These results indicate that the parameters of PR-IHPS are tuned appropriately after parameter

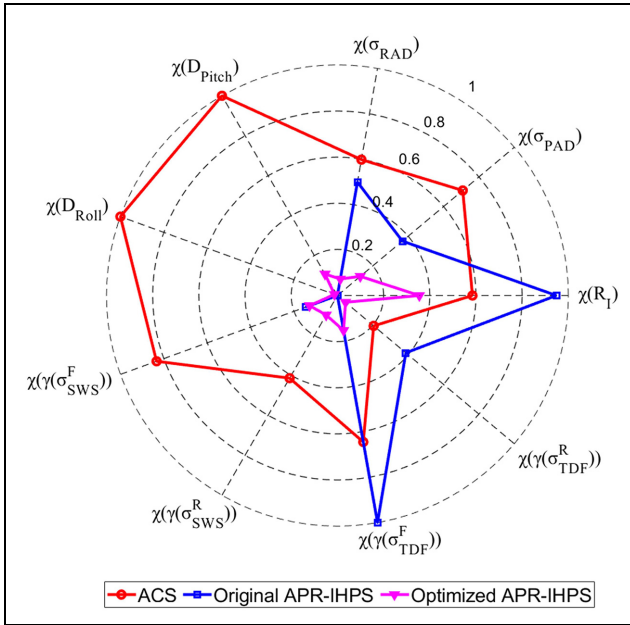


Figure 14. Comparison of the evaluation indexes. The normalization factor $\chi(\bullet)$ can be formulated as $\chi(\bullet) = [\bullet - \min(\bullet)] / [\max(\bullet) - \min(\bullet)]$, in which \bullet is a normalized evaluation index, that is, R_l , and \bullet is the column vector composed of all R_l in the workable region. That $\chi(\bullet)$ is equal to either 1 or 0, which indicates the maximum or minimum of the evaluation index.

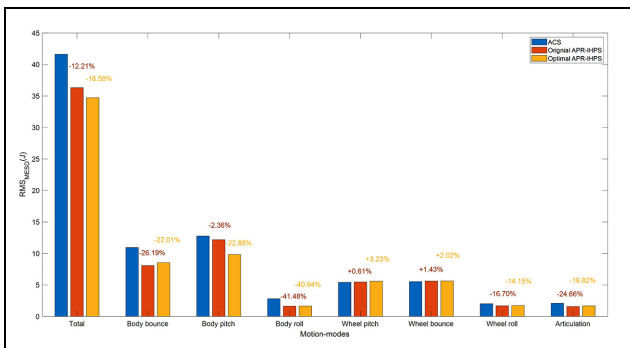


Figure 15. Comparison of RMS values of MESD.

optimization, so that all performance indexes are greatly improved. It should be noted that the articulation MESD still remains low after parameter optimization, which indicates that the tires can keep good road holding ability for an off-road condition. In addition, the hydraulic actuator forces are compared to investigate the power consumption of the hydraulic actuator. Figure 16 indicates that the actuator forces after the optimization become much smaller, which corresponds to the fact that the power consumption of the actuator is also optimized.

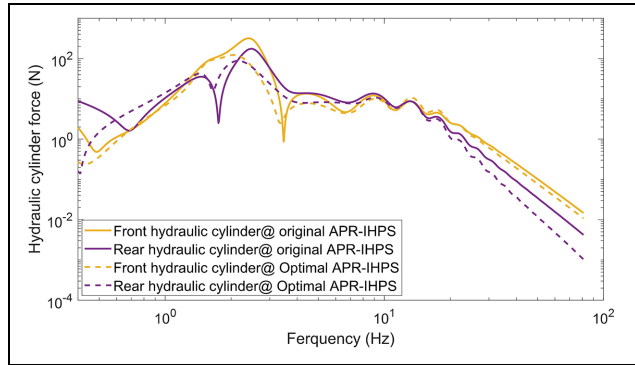


Figure 16. Comparison of hydraulic forces under different design parameters.

Conclusion

In this study, a PR-IHPS system has been presented to improve both pitch and roll dynamics for ambulances to meet the requirements of stability and ride comfort. The coupled dynamic equations of APR-IHPS system have been derived using impedance transfer matrix method. Based on the coupled equations, the characteristics of PR-IHPS system are quantitatively analyzed, which indicates that the additional stiffness mainly depends on the capacities of accumulators and cross-sectional areas of hydraulic cylinders. When the front and rear cylinders of the same size are oppositely installed, only the pitch and roll stiffness for vehicle body are provided by PR-IHPS system, while the bounce-stiffness is not provided. The additional damping characteristics can be determined by adjusting the loss coefficients of damper valves. Particularly, the damping of pitch and roll motions for vehicle body can be controlled by tuning the loss coefficients of ADVs.

In addition, a MESD method is proposed which can obtain the vibration energy for each motion-mode in frequency domain. Then, the parametric design approach for PR-IHPS is also presented based on the proposed MESD method. The desirable parameters of PR-IHPS system are obtained by the parametric design approach taking both ride comfort and handling performance into consideration. The simulation results show that (1) minimal bounce-stiffness and large pitch/roll stiffness could be achieved by the design of cylinder area ratios, (2) the design range for capacity of accumulator could be determined to have a reasonably distribution of stiffness between pitch and roll motion, and (3) the overall performance for the lying patient can be significantly improved by the parameter optimization of the PR-IHPS system. For future work, one task for our ongoing researches is evaluation of handling performance on time domain transient responses with respect to emergency braking and steering. In addition, implementation and validation of the proposed

approach including both suspension subsystem and complete system-level field testing will be conducted.


Declaration of conflicting interests


The author(s) declared no potential conflicts of interest with respect to the research, authorship, and/or publication of this article.

Funding

The author(s) disclosed receipt of the following financial support for the research, authorship, and/or publication of this article: Some of the work presented herein was partially funded by Chinese National Natural Science Foundation (grant no. 51675152) and Hunan Provincial Science Foundation of China (grant no. 2017JJ2031). Any opinions, findings, and conclusions or recommendations expressed in this material are those of the authors and do not necessarily reflect the views of the particular funding agency. The authors are grateful for the support obtained.

ORCID iDs

Bohuan Tan  <https://orcid.org/0000-0002-2561-8793>

Nong Zhang  <https://orcid.org/0000-0002-8051-4946>

References

- Mustafa C, Ceyhan B, Sertac Y, et al. Effects of whole body vibration training on isokinetic muscular performance, pain, function, and quality of life in female patients with patellofemoral pain: a randomized controlled trial. *J Musculoskel Neuron* 2018; 18: 473–484.
- Chen Y, Zhang B, Zhang N, et al. A condensation method for the dynamic analysis of vertical vehicle–track interaction considering vehicle flexibility. *J Vib Acoust* 2015; 137: 041010.
- Inan OT, Etemadi M, Widrow B, et al. Adaptive cancellation of floor vibrations in standing ballistocardiogram measurements using a seismic sensor as a noise reference. *IEEE Trans Biomed Eng* 2010; 57: 722–727.
- Sagawa K, Inooka H, Ino-oka E, et al. On an ambulance stretcher suspension concerned with the reduction of patient's blood pressure variation. *Proc Inst Mech Eng Part H* 1997; 211: 199–208.
- Zhou JX, Wang K, Xu DL, et al. Vibration isolation in neonatal transport by using a quasi-zero-stiffness isolator. *J Vib Control* 2018; 24: 3278–3291.
- Abdelkareem MAA, Xu L, Guo XX, et al. Energy harvesting sensitivity analysis and assessment of the potential power and full car dynamics for different road modes. *Mech Syst Sig Process* 2018; 110: 307–332.
- Zhao W and Zhang H. Coupling control strategy of force and displacement for electric differential power steering system of electric vehicle with motorized wheels. *IEEE Trans Veh Technol* 2018; 67: 8118–8128.
- Xiao P, Gao H, Shi PC, et al. Research on air suspension with novel dampers based on glowworm swarm optimization proportional-integral-derivative algorithm. *Adv Mech Eng*. Epub ahead of print 3 August 2018. DOI: 10.1177/1687814018791710
- Yang M, Xu X, Su W, et al. The dynamic performance optimization for nonlinear vibration-reduction system of the tracked ambulance. *Proc IMechE, Part C: J Mechanical Engineering Science* 2015; 229: 2719–2729.
- Xu X, Yang M, Jia ND, et al. The structure optimization of tracked ambulance nonlinear vibration reduction system. *J Mech Sci Technol* 2017; 31: 523–533.
- Yang M, Xu XX and Su C. A study on vibration characteristics and stability of the ambulance nonlinear damping system. *Abstr Appl Anal* 2013; 2013: 501081.
- Xu XX, Wang M, Cui XD, et al. Simulation analysis and optimization design for vibration damping of stretchers on emergency ambulance. *J Vib Eng* 2009; 22: 352–356.
- Pan GY and Zhang Y. Study on ambulance stretcher vibration isolation system. *Int Conf Vib Struct Eng Meas* 2012; 226: 324.
- Prehn J, McEwen I, Jeffries L, et al. Decreasing sound and vibration during ground transport of infants with very low birth weight. *J Perinatol* 2014; 35: 110–114.
- Raine JK and Henderson RJ. A two-degree-of-freedom ambulance stretcher suspension: simulation of system performance with capillary and orifice pneumatic damping. *Proc IMechE, Part D: J Automobile Engineering* 1998; 21: 227–240.
- Sagawa K and Inooka H. Ride quality evaluation of an actively-controlled stretcher for an ambulance. *Proc IMechE, Part H: J Engineering in Medicine* 2002; 216: 247–256.
- Chae HD and Choi SB. A new vibration isolation bed stage with magnetorheological dampers for ambulance vehicles. *Smart Mater Struct* 2015; 24: 017001.
- Zou JY, Guo XX, Xu L, et al. Design, modeling, and analysis of a novel hydraulic energy-regenerative shock absorber for vehicle suspension. *Shock Vib* 2017; 2017: 3186584.
- Shaer B, Kenne JP, Kaddissi C, et al. Real-time hybrid control of electrohydraulic active suspension. *Int J Robust Nonlin* 2018; 27: 4968–4991.
- Huang Y, Na J, Wu X, et al. Approximation-free control for vehicle active suspensions with hydraulic actuator. *IEEE Trans Indus Electr* 2018; 65: 7258–7267.
- Zhao W, Wang Y and Wang C. Multidisciplinary optimization of electric-wheel vehicle integrated chassis system based on steady endurance performance. *J Clean Product* 2018; 186: 640–651.
- Wang KY, He P, Tang JH, et al. Static output feedback H-infinity control for active suspension system with input delay and parameter uncertainty. *Adv Mech Eng*. Epub ahead of print 2 July 2018. DOI: 10.1177/1687814018786581
- Makowski M and Knap L. Investigation of an off-road vehicle equipped with magnetorheological dampers. *Adv Mech Eng*. Epub ahead of print 28 May 2018. DOI: 10.1177/1687814018778222
- Zhang B, Zhang J and Yi J. Modal and dynamic analysis of a vehicle with kinetic dynamic suspension system. *Shock Vib* 2016; 2016: 1–18.
- Wu Y and Zhang N. Modeling and performance analysis of a vehicle with kinetic dynamic suspension system. *Proc*

- IMechE, Part D: J Automobile Engineering* 2019; 233: 697–709.
26. Cao D, Rakheja S and Su C. Dynamic analyses of heavy vehicle with pitch-interconnected suspensions. *Int J Heavy Veh Syst* 2008; 15: 272–308.
 27. Zhang N, Smith WA and Jeyakumar J. Hydraulically interconnected vehicle suspension: background and modelling. *Veh Syst Dyn* 2008; 48: 17–40.
 28. Smith WA and Zhang N. Hydraulically interconnected vehicle suspension: optimization and sensitivity analysis. *Proc IMechE, Part D: J Automobile Engineering* 2010; 224: 1335–1355.
 29. Qi H, Zhang B, Zhang N, et al. Enhanced lateral and roll stability study for a two-axle bus via hydraulically interconnected suspension tuning. *SAE Int J Veh* 2019, <https://www.sae.org/publications/technical-papers/content/10-03-01-0001/>
 30. Ding F, Zhang N, Liu J, et al. Dynamics analysis and design methodology of roll-resistant hydraulically interconnected suspensions for tri-axle straight trucks. *J Frank Ins* 2016; 353: 4620–4651.
 31. Tan B, Wu Y, Zhang N, et al. Dynamic characteristics analysis of an ambulance with hydraulically interconnected suspension system. SAE technical paper 2018-01-0815, 2018.
 32. Shao X. Modeling and model analysis of a full-car fitted with an anti-pitch anti-roll hydraulically interconnected suspension. SAE technical paper 2014-01-0849, 2014.
 33. Zhang N, Wang L and Du H. Motion-mode energy method for vehicle dynamics analysis and control. *Veh Syst Dyn* 2014; 52: 1–25.
 34. Wang L, Zhang N and Du H. Real-time identification of vehicle motion-modes using neural networks. *Mech Syst Signal Pr* 2015; 50: 632–645.
 35. Chen Y, Dagny J and Peter A. Underwater dynamic response at limited points expanded to full-field strain response. *J Vib Acoust* 2018; 140: 051016.
 36. Zheng M, Peng P, Zhang B, et al. A new physical parameter identification method for two-axis on-road vehicles: simulation and experiment. *Shock Vib* 2015; 2015: 191050.
 37. ISO 2631. *Mechanical vibration and shock-evaluation of human exposure to whole-body vibration—part 1: general requirements*. Geneva: International Organization for Standardization, 1997.
 38. Chen YC, Zhang BJ and Chen SZ. Model reduction technique tailored to the dynamic analysis of a beam structure under a moving load. *Shock Vib* 2014; 2014: 406093.
 39. David JM and Sampson David C. Active roll control of single unit heavy road vehicles. *Veh Syst Dyn* 2003; 40: 229–270.

Appendix I

Notation

- a, b longitudinal distance from CG of vehicle body to the front wheel stations and rear pivot centers, respectively

- c_{sij} suspension linear damping coefficients for ACS systems ($i = f, r; j = l, r$)
- C_a capacity of gas-filled diaphragm accumulator
- D_0, F_0 suspension static deformation and tire static force
- D_{Pitch}, D_{Roll} MESDs of pitch and roll modes
- $H(f)_{\ddot{y}-q}$ TF from road displacement input to acceleration response of sprung mass
- I_p, R_p, C_p liquid inductance, liquid resistance, and liquid capacitance of pipeline fluid element, respectively
- I_θ pitch inertia of sprung mass around center of gravity of itself
- I_ϕ roll inertia of sprung mass around center of gravity of itself
- k_{sij} suspension linear stiffness coefficients for ACS systems ($i = f, r; j = l, r$)
- k_{ij} tire linear stiffness coefficients for ACS systems ($i = f, r; j = l, r$)
- k_{ARBi} torsional linear stiffness coefficients of ARBs for ACS systems ($i = f, r$)
- m_s mass of sprung mass
- m_{tij} mass of unsprung mass ($i = f, r; j = l, r$)
- $\mathbf{M}_D, \mathbf{K}_D$ equivalent mass coefficient and stiffness coefficient vectors
- P, Q mean pressure and flow in pipeline fluid element, respectively
- P_i, Q_i up-stream pressure/flow and down-stream pressure/flow ($i = U, D$)
- P_{ijT}, P_{ijB} pressure in the piston head chamber and piston rod chamber of cylinder chamber, respectively ($i = f, r; j = l, r$)
- P_p, V_p pre-charged pressure and gas volume in accumulator
- Q_{ijT}, Q_{ijB} flow in the piston head chamber and piston rod chamber of cylinder chamber, respectively ($i = f, r; j = l, r$)
- R_I RMS value of WARP calculated by ISO 2631
- S_{ijT}, S_{ijB} effective cross-sectional area for top and bottom cylinders, respectively ($i = f, r; j = l, r$)
- t_i transverse distance of vehicle body from CG of vehicle body to wheel stations ($i = f, r$)
- \mathbf{T}_j transformation matrix of the j th order motion-mode ($j = 1, 2, \dots, 7$)
- ${}^{kj}\mathbf{T}_{ki}^v, {}^{kj}\mathbf{T}_{ki}^p, {}^{kj}\mathbf{T}_{ki}^t$ impedance matrices for damper valve, pipeline, and ATJDV components in k th circuit from up-stream i to down-stream j
- $\mathbf{Y}_j^V, \mathbf{Y}_j^D$ velocity and elastic deformation PSD response vectors in j th motion-mode
- z_{gij} road disturbance inputs at wheel–road contact points ($i = f, r; j = l, r$)

Z_s	sprung mass vertical displacement	θ	pitch angle displacement of sprung mass
Z_{uij}	unsprung mass vertical displacement ($i = f, r; j = l, r$)	μ	pitch angle displacement of sprung mass around center of gravity of itself
$Z_A, Z_H,$ Z_R	pressure loss coefficients of the ADV, PHDV, and PRDV, respectively	$\sigma_{SWS},$ σ_{TDF}	cross-sectional area ratio between the rear and front top cylinders
$Z_{PR-IHPS}$	additional characteristic matrix generated by the PR-IHPS system	$\sigma_{PAD},$ σ_{RAD}	RMS value in terms of SWS and TDF
$\gamma(\sigma_{SWS})$	dynamic SWS coefficient	ϕ	RMS value in terms of PAD and RAD
$\gamma(\sigma_{TDF})$	dynamic TDF coefficient	$\chi(\bullet)$	roll angle displacement of sprung mass around center of gravity of itself
η_i	cross-sectional area ratio between the bottom and top of the front or rear cylinder ($i = f, r$)		normalization factor for specified index, that is, $\chi(R_I), \chi(\sigma_{PAD})$

Appendix 2 The parameters of vehicle and PR-IHPS system.

Conventional ambulance				Pitch–roll-interconnected hydro-pneumatic suspension (PR-IHPS)			
Symbol	Value	Symbol	Value	Symbol	Value	Symbol	Value
m_s	$3.5 \times 10^3 \text{ kg}$	k_{srl}/k_{srr}	$1.17 \times 10^5 \text{ N m}^{-1}$	ρ	$8.7 \times 10^2 \text{ kg m}^{-3}$	V_p	$6.3 \times 10^{-4} \text{ m}^3$
I_θ	$6.5 \times 10^3 \text{ kg m}^2$	c_{sfl}/c_{sfr}	$2.2 \times 10^3 \text{ N s m}^{-1}$	μ	$5 \times 10^{-2} \text{ N s m}^{-2}$	P_p	0.5 MPa
I_ϕ	$1.9 \times 10^3 \text{ kg m}^2$	c_{srl}/c_{srr}	$2.6 \times 10^3 \text{ N s m}^{-1}$	B	$1.4 \times 10^3 \text{ MPa}$	P	1.8 MPa
m_{tfl}/m_{tfr}	45 kg	$k_{tfl}/k_{tfr}/k_{trl}/k_{trr}$	$3.7 \times 10^5 \text{ N m}^{-1}$	r_p	$1 \times 10^{-2} \text{ m}$	Z_H	$7 \times 10^8 \text{ kg s}^{-1} \text{ m}^{-4}$
m_{trf}/m_{trr}	50 kg	k_{ARbf}	$6 \times 10^4 \text{ N rad}^{-1}$	t_p	$1 \times 10^{-2} \text{ m}$	Z_R	$7 \times 10^8 \text{ kg s}^{-1} \text{ m}^{-4}$
k_{sfl}/k_{sfr}	$1.17 \times 10^5 \text{ N m}^{-1}$	k_{ARBr}	$4.5 \times 10^4 \text{ N rad}^{-1}$	E	$2.1 \times 10^2 \text{ GPa}$	Z_A	$3 \times 10^8 \text{ kg s}^{-1} \text{ m}^{-4}$
a	1.78 m	t_f	0.64 m	D_T	$5 \times 10^{-2} \text{ m}$		
b	1.32 m	t_r	0.64 m	D_B	$4 \times 10^{-2} \text{ m}$		

Appendix 3 Natural frequencies and mode shape comparison between ACS and APR-IHPS.

Mode		Body bounce	Body roll	Body pitch	Wheel pitch	Wheel bounce	Wheel roll	Articulation
Ambulance with conventional suspension (ACS)								
f (Hz)	1.527	1.546		1.897	15.576	16.514	17.349	18.936
ξ	0.084	0.047		0.086	0.272	0.243	0.241	0.208
Z_s	0	0		-0.615-0.041i	-0.010-0.012i	-0.009-0.009i	0	0
θ	0.332-0.018i	0		0	-0.007-0.008i	0.008 + 0.009i	0	0
ϕ	0	0		0	0	0	-0.014-0.011i	0.012 + 0.008i
Z_{ufr}	0.097 + 0.022i	0.224 + 0.014i		-0.582-0.090i	-0.011 + 0.010i	0	0.006-0.029i	-1
Z_{ufr}	0.094 + 0.022i	-0.224-0.014i		-0.582-0.090i	-0.011 + 0.010i	0	-0.006 + 0.029i	1
Z_{urr}	0.337 + 0.053i	0.207 + 0.019i		0.163 + 0.044i	0	0.011-0.009i	0	0.009-0.024i
Z_{urr}	0.337 + 0.053i	-0.207-0.019i		0.163 + 0.044i	0	0.011-0.009i	0	-0.009 + 0.024i
Ambulance with pitch-roll-interconnected hydro-pneumatic suspension (APR-IHPS)								
f (Hz)	1.606	1.869		2.509	16.041	13.392	16.275	13.774
ξ	0.202	0.113		0.151	0.795	0.576	0.771	0.567
Z_s	0	0		-0.192 + 0.071i	-0.015 + 0.051i	-0.024 + 0.050i	0	0
θ	0.098-0.025i	0		0	0.041-0.030i	-0.008-0.000i	0	0
ϕ	0	0		0	0	0	-0.052 + 0.043i	-0.017 + 0.007i
Z_{ufr}	0.166-0.065i	0.276-0.062i		-0.773 + 0.288i	0	0.655-0.170i	0	-0.651 + 0.234i
Z_{ufr}	0.166-0.065i	-0.276 + 0.062i		-0.773 + 0.288i	0	0.655-0.170i	0	0.651-0.234i
Z_{urr}	0.280-0.130i	0.272-0.067i		0.580-0.136i	-0.542 + 0.122i	0	0.552-0.168i	1
Z_{urr}	0.280-0.130i	-0.272 + 0.067i		0.580-0.136i	-0.542 + 0.122i	0	-0.552 + 0.168i	-1